**51st AIAA/ASME/ASCE/AHS/ASC Structures, Structural Dynamics, and Materials Conference
 18th 12 - 15 April 2010, Orlando, Florida**

AIAA 2010-3032

An Improved Beam Formulation for Aeroelastic Applications

Alberto Varello[*]

Politecnico di Torino, Torino, Italy

San Diego State University, San Diego, CA 92182-1308

Luciano Demasi[‡]

San Diego State University, San Diego, CA 92182-1308

Erasmo Carrera[‡]

Politecnico di Torino, Torino, Italy

Gaetano Giunta[§]

Centre de Recherche Public Henri Tudor, Luxembourg-Kirchberg, Luxembourg

A refined beam model for the linear static aeroelastic analysis of generally oriented lifting systems is described in this paper. It is aimed at beam-like structures such as classical and unconventional wing configurations. The structural formulation of refined beam finite elements is embedded in the framework of Carrera Unified Formulation. Increasing accuracy in predicting effects of warping, in-plane deformation is obtained by considering as a free parameter the order of the displacement field expansion over the cross-section. Linear steady aerodynamic loads are described via the Vortex Lattice Method and the transfer to their energetically equivalent structural loads is performed by the Principle of Virtual Displacements. Thanks to the accuracy of refined elements, the coupling of structural and aerodynamic fields is performed via the Infinite Plate Spline method. The procedure involves a set of pseudo-structural points placed on the reference surface of the wing system. Different beam elements as well as different higher-order models are considered for the analysis of various cross-section geometries and loading cases. The structural results are validated with benchmarks retrieved from the classical models and NASTRAN. Aeroelastic results show well correspondence with NASTRAN results for a number of wing configurations. The proposed higher-order model proves its increasing accuracy in predicting aeroelastic responses with respect to analyses based on classical beam theories.

I.   Introduction

IN recent years a push towards the design optimization, aerodynamic and structural understanding of unconventional wing configurations such as Joined Wings and C-Wings has occurred. Although they have been examined thoroughly for almost the last 30 years,[1−3] their aeroelastic behavior and effect on design are still not completely comprehended.[4]

Such a kind of wing systems finds applications extending from civil transport to military field. For instance, the development of Unmanned Aerial Vehicles (UAVs) has led to the birth of the "sensorcraft". Sensorcraft is a joined wing aircraft designed for long-range, high-altitude intelligence, surveillance and reconnaissance. Whereas, as far as the box plane is concerned, a study based on PrandtlPlane concept for a 250-300 seat civil transport aircraft was completed for Airbus Deutschland in 2007. Then a static model

---

[*]PhD student, Aeronautics and Space Engineering Department, Politecnico di Torino. Visiting scholar, Department of Aerospace Engineering and Engineering Mechanics, San Diego State University.

[†]Assistant Professor, Department of Aerospace Engineering and Engineering Mechanics, Member AIAA.

[‡]Professor, Aeronautics and Space Engineering Department, Member AIAA.

[§]Research Scientist, Department of Advanced Materials and Structures, Member AIAA.

American Institute of Aeronautics and Astronautics

of PrandtlPlane designed for Bauhaus Luftfahrt was presented during the Berlin Air Show in May 2008. Again, aeroelastic investigations of geometrically nonlinear lifting surfaces in the past few years covered high-aspect ratio wings of High-Altitude Long-Endurance aircraft[5,6] (HALE), strut-braced wings,[7,8] truss-braced wings,[9] wind tunnel models of delta, beam-like wings and C-Wing configurations.[10]

Practically, beam-like structures can be analyzed by means of beam theories. Hodges[11] developed a relevant example of geometrically exact structural beam model for the dynamics of beam-like structures. However, higher-order beam elements are required in engineering fields such as aeroelasticity where the proper analysis of torsional and bending vibration modes is fundamental to predict aeroelastic responses as well as critical phenomena. Refined theories are necessary to cope with unconventional cross-section geometries, short beams, orthotropic materials and non-homogenous sections.

A review of several beam and plate theories for vibration, wave propagations, buckling and post-buckling was presented by Kapania and Raciti.[12,13] Particular attention was given to models that account for transverse shear-deformation. Moreover, a review about the developments in finite element formulations for thin and thick laminated beams was provided. Kim and White[14] investigated non-classical effects in composite box beam models, such as torsional warping and transverse shear effects. Third-order, locking free beam element was developed by Reddy,[15] where Euler-Bernoulli's and Timoshenko's models were obtained as special cases of the proposed element. Lee[16] studied the flexural-torsional behavior of I-shaped composite beams. Transverse shear deformation, coupling and warping effects were accounted for.

Refined theories are also developed by exploiting the asymptotic method. A suitable kinematics model for a structural problem is obtained by investigating the role played by the various variables in terms of a perturbation parameter (usually a geometrical one such as the span-to-height ratio for beams). The 3D problem is then reduced to a 1D model by utilizing an asymptotic series of a characteristic parameter and retaining those terms which exhibit the same order of magnitude when the perturbation parameter vanishes. Relevant contributions in developing higher-order beam theories via asymptotic methods are represented by VABS.[17−19]

In this paper the aeroelastic and structural formulations of refined beam finite elements are addressed. The proposed structural formulation is embedded in the framework of Carrera Unified Formulation (CUF).[29] CUF offers a systematic procedure to obtain refined structural models by considering the order of the theory as a free parameter of the formulation. Different beam elements (with 2, 3 and 4 nodes) as well as different higher-order models for the cross-section displacements field are used. Euler-Bernoulli's and Timoshenko's beam models are obtained as particular cases of the first-order formulation. The beam cross-section has been considered rectangular or square and the material is isotropic. The structural results are validated with benchmarks retrieved from the classical models and NASTRAN. The proposed aeroelastic formulation is based on the work of Demasi and Livne.[10,32] The aeroelastic assessment consists in the comparison of results with NASTRAN for several straight and swept wings.

II.   Preliminaries

A beam is a structure whose axial extension l is predominant respect to any other dimension orthogonal to it. By intersecting the beam with a plane perpendicular to its axis the beam's cross-section Ω is identified, as shown in Fig. 1. The Cartesian coordinate system is composed of x and z axes parallel to the cross-section plane, whereas the y direction outreaches along the beam axis and is bounded so that $0 \leq y \leq l$. In general, the origin O can lie outside the contour of the cross-section, which is considered to be constant along the beam axis identified by the y coordinate. The notation for the displacement vector is:

$$\boldsymbol{u}\left(x,\,y,\,z\right) = \left\{ \begin{matrix} u_x & u_y & u_z \end{matrix} \right\}^T \tag{1}$$

The stress and strain vectors are split into the terms on the cross-section:

$$\boldsymbol{\sigma}_n = \left\{ \begin{matrix} \sigma_{zy} & \sigma_{xy} & \sigma_{yy} \end{matrix} \right\}^T \qquad \boldsymbol{\varepsilon}_n = \left\{ \begin{matrix} \varepsilon_{zy} & \varepsilon_{xy} & \varepsilon_{yy} \end{matrix} \right\}^T \tag{2}$$

and the terms lying on planes orthogonal to the cross-section:

$$\boldsymbol{\sigma}_p = \left\{ \begin{matrix} \sigma_{zz} & \sigma_{xx} & \sigma_{zx} \end{matrix} \right\}^T \qquad \boldsymbol{\varepsilon}_p = \left\{ \begin{matrix} \varepsilon_{zz} & \varepsilon_{xx} & \varepsilon_{zx} \end{matrix} \right\}^T \tag{3}$$

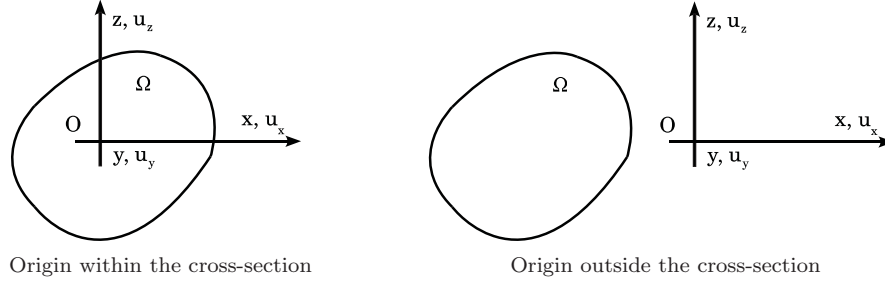American Institute of Aeronautics and Astronautics

Figure 1. Beam's cross-section geometry and coordinate system.

In the case of small displacement with respect to a characteristic dimension of the cross-section Ω, the following linear relations between strain and displacement components hold:

$$\varepsilon_n = \left\{ u_{z,y} + u_{y,z} \quad u_{x,y} + u_{y,x} \quad u_{y,y} \right\}^T \qquad \varepsilon_p = \left\{ u_{z,z} \quad u_{x,x} \quad u_{z,x} + u_{x,z} \right\}^T \qquad (4)$$

The subscripts x, y and z preceded by comma represent the derivatives with respect to the spatial coordinates. A compact vectorial notation can be adopted:

$$\begin{aligned} \varepsilon_n &= \boldsymbol{D}_{np}\, \boldsymbol{u} + \boldsymbol{D}_{ny}\, \boldsymbol{u} \\ \varepsilon_p &= \boldsymbol{D}_p\, \boldsymbol{u} \end{aligned} \qquad (5)$$

where $\boldsymbol{D}_{np}$, $\boldsymbol{D}_{ny}$, and $\boldsymbol{D}_p$ are differential matrix operators:

$$\boldsymbol{D}_{np} = \begin{bmatrix} 0 & \dfrac{\partial}{\partial z} & 0 \\ 0 & \dfrac{\partial}{\partial x} & 0 \\ 0 & 0 & 0 \end{bmatrix}, \quad \boldsymbol{D}_{ny} = \begin{bmatrix} 0 & 0 & \dfrac{\partial}{\partial y} \\ \dfrac{\partial}{\partial y} & 0 & 0 \\ 0 & \dfrac{\partial}{\partial y} & 0 \end{bmatrix}, \quad \boldsymbol{D}_p = \begin{bmatrix} 0 & 0 & \dfrac{\partial}{\partial z} \\ \dfrac{\partial}{\partial x} & 0 & 0 \\ \dfrac{\partial}{\partial z} & 0 & \dfrac{\partial}{\partial x} \end{bmatrix} \qquad (6)$$

In the case of beams made of linear elastic orthotropic materials, the generalized Hooke's law holds:

$$\boldsymbol{\sigma} = \boldsymbol{C}\,\boldsymbol{\varepsilon} \qquad (7)$$

According to Eqs. 2 and 3, the previous expression becomes:

$$\begin{aligned} \boldsymbol{\sigma}_p &= \widetilde{\boldsymbol{C}}_{pp}\,\varepsilon_p + \widetilde{\boldsymbol{C}}_{pn}\,\varepsilon_n \\ \boldsymbol{\sigma}_n &= \widetilde{\boldsymbol{C}}_{np}\,\varepsilon_p + \widetilde{\boldsymbol{C}}_{nn}\,\varepsilon_n \end{aligned} \qquad (8)$$

where matrices $\widetilde{\boldsymbol{C}}_{pp}$, $\widetilde{\boldsymbol{C}}_{pn}$, $\widetilde{\boldsymbol{C}}_{np}$ and $\widetilde{\boldsymbol{C}}_{nn}$ are:

$$\widetilde{\boldsymbol{C}}_{pp} = \begin{bmatrix} \widetilde{C}_{11} & \widetilde{C}_{12} & \widetilde{C}_{16} \\ \widetilde{C}_{12} & \widetilde{C}_{22} & \widetilde{C}_{26} \\ \widetilde{C}_{16} & \widetilde{C}_{26} & \widetilde{C}_{66} \end{bmatrix}, \quad \widetilde{\boldsymbol{C}}_{pn} = \widetilde{\boldsymbol{C}}_{np}^T = \begin{bmatrix} 0 & 0 & \widetilde{C}_{13} \\ 0 & 0 & \widetilde{C}_{23} \\ 0 & 0 & \widetilde{C}_{36} \end{bmatrix}, \quad \widetilde{\boldsymbol{C}}_{nn} = \begin{bmatrix} \widetilde{C}_{55} & \widetilde{C}_{45} & 0 \\ \widetilde{C}_{45} & \widetilde{C}_{44} & 0 \\ 0 & 0 & \widetilde{C}_{33} \end{bmatrix} \qquad (9)$$

For the sake of brevity, the dependence of the coefficients $\widetilde{C}_{ij}$ on Young's moduli, Poisson's ratios, shear moduli and the fibre angle is not reported here. It can be found in Reddy[21] or Jones.[22]

III.   Refined Beam Theory

According to the framework of Carrera Unified Formulation[20] (CUF), the displacement field is assumed as an expansion of a certain class of functions F_τ, which depends on the cross-section coordinates x and z:

$$\boldsymbol{u}(x, y, z) = F_\tau(x, z)\,\boldsymbol{u}_\tau(y) \qquad \tau = 1,\, 2,\, \ldots,\, N_u = N_u(N) \qquad (10)$$

American Institute of Aeronautics and Astronautics

The compact expression is based on the Einstein's notation: repeated subscript τ indicates summation. The number of expansion terms N_u depends on the expansion order N, which is a free parameter of the formulation and at maximum equal to 4 in the present work. Mac Laurin's polynomials are chosen as cross-section functions F_τ and are listed in Table 1.

N	N_u	F_τ
0	1	$F_1 = 1$
1	3	$F_2 = x \quad F_3 = z$
2	6	$F_4 = x^2 \quad F_5 = xz \quad F_6 = z^2$
3	10	$F_7 = x^3 \quad F_8 = x^2z \quad F_9 = xz^2 \quad F_{10} = z^3$
$\vdots$	$\vdots$	$\vdots$
N	$\frac{(N+1)(N+2)}{2}$	$F_{\frac{(N^2+N+2)}{2}} = x^N \quad F_{\frac{(N^2+N+4)}{2}} = x^{N-1}z \quad \ldots \quad F_{\frac{N(N+3)}{2}} = xz^{N-1} \quad F_{\frac{(N+1)(N+2)}{2}} = z^N$

Table 1. **Number of expansion terms and Mac Laurin's polynomials as function of N.**

Most displacement-based theories can be formulated on the basis of the above generic kinematic field. For instance, when $N = 3$, the third-order axiomatic displacement field is given by:

$$
\begin{aligned}
u_x &= u_{x1} + u_{x2}\,x + u_{x3}\,z + u_{x4}\,x^2 + u_{x5}\,xz + u_{x6}\,z^2 + u_{x7}\,x^3 + u_{x8}\,x^2z + u_{x9}\,xz^2 + u_{x10}\,z^3 \\
u_y &= u_{y1} + u_{y2}\,x + u_{y3}\,z + u_{y4}\,x^2 + u_{y5}\,xz + u_{y6}\,z^2 + u_{y7}\,x^3 + u_{y8}\,x^2z + u_{y9}\,xz^2 + u_{y10}\,z^3 \\
u_z &= u_{z1} + u_{z2}\,x + u_{z3}\,z + u_{z4}\,x^2 + u_{z5}\,xz + u_{z6}\,z^2 + u_{z7}\,x^3 + u_{z8}\,x^2z + u_{z9}\,xz^2 + u_{z10}\,z^3
\end{aligned}
\tag{11}
$$

Then the classical beam models, such as Timoshenko[23] (TBM) and Euler-Bernoulli (EBBM), are derived in ease from the first-order approximation model:

$$
\begin{aligned}
u_x &= u_{x1} + u_{x2}\,x + u_{x3}\,z \\
u_y &= u_{y1} + u_{y2}\,x + u_{y3}\,z \\
u_z &= u_{z1} + u_{z2}\,x + u_{z3}\,z
\end{aligned}
\tag{12}
$$

Timoshenko's beam model (TBM) can be obtained by modifying the cross-section functions F_τ; in particular the terms $\{\,u_{ij} : i = x, z\,;\, j = 2, 3\,\}$ are set equal to zero. In addiction, for EBBM an infinite rigidity in the transverse shear is also adopted by penalizating ε_{xy} and ε_{yz}.

Higher-order models provide an accurate description of the shear mechanics, the cross-section deformations, the coupling of the spatial directions due to Poisson's effect and the torsional mechanics more in detail than classical models do. The EBBM neglects them all, since it was formulated to describe the bending mechanics. The TBM accounts for constant shear stress and strain components. Classical theories and first-order models require the assumption of opportunely reduced material stiffness coefficients $\widetilde{C}_{ij}$ to correct the Poisson's locking effect.[24−26]

IV.   Finite Element Formulation

Following standard FEM, the unknown variables in the element domain are expressed in terms of their values corresponding to the element nodes.[27,28] By introducing the shape functions N_i and the nodal displacement vector $\boldsymbol{q}$, the displacement field becomes:

$$
\boldsymbol{u}\,(x,\,y,\,z) = F_\tau\,(x,\,z)\,N_i\,(y)\,\boldsymbol{q}_{\tau i} \qquad i = 1,\,2,\,\ldots,\,N_N
\tag{13}
$$

where:

$$
\boldsymbol{q}_{\tau i} = \left\{\,q_{u_{x\tau i}} \quad q_{u_{y\tau i}} \quad q_{u_{y\tau i}}\,\right\}^T
\tag{14}
$$

contains the degrees of freedom of the τ-th expansion term corresponding to the i-th element node. Elements with number of nodes N_N equal to 2, 3 and 4 are formulated and addressed as B2, B3, B4 respectively.[29,30]

American Institute of Aeronautics and Astronautics

For the sake of brevity, their shape functions are not reported here, since they can be found in Bathe.[31] The stiffness matrix of finite element and the external loads coherent to the model are obtained via the Principle of Virtual Displacements:

$$\delta L_{int} = \int_V \left(\delta \boldsymbol{\varepsilon}_n^T \boldsymbol{\sigma}_n + \delta \boldsymbol{\varepsilon}_p^T \boldsymbol{\sigma}_p \right) dV = \delta L_{ext} \tag{15}$$

where L_{int} is the strain energy, L_{ext} stands for the work of external loads and δ indicates the virtual variation. Since the cross-section functions F_τ are not dependent on y, the strain vectors can be written by coupling Eqs. 5 and 13:

$$\begin{aligned} \boldsymbol{\varepsilon}_n &= \left(\boldsymbol{D}_{np} F_\tau \boldsymbol{I} \right) N_i \boldsymbol{q}_{\tau i} + F_\tau \left(\boldsymbol{D}_{ny} N_i \boldsymbol{I} \right) \boldsymbol{q}_{\tau i} \\ \boldsymbol{\varepsilon}_p &= \left(\boldsymbol{D}_p F_\tau \boldsymbol{I} \right) N_i \boldsymbol{q}_{\tau i} \end{aligned} \tag{16}$$

By substituting the previous expression in Eq. 15 and using Eq. 8, the virtual variation is written in a compact notation depending on the virtual variation of nodal displacements:

$$\delta L_i = \delta \boldsymbol{q}_{\tau i}^T \boldsymbol{K}^{ij\tau s} \boldsymbol{q}_{sj} \tag{17}$$

The matrix $\boldsymbol{K}^{ij\tau s}$ has dimension 3×3 and is the *fundamental nucleus* of the Structural Stiffness Matrix. For the sake of brevity, it is shown how to compute only the $K_{yz}^{ij\tau s}$ component, for instance:

$$\begin{aligned} K_{yz}^{ij\tau s} = \; & \widetilde{C}_{55} \int_\Omega F_{\tau,z} F_s \, d\Omega \int_l N_i N_{j,y} \, dy + \widetilde{C}_{45} \int_\Omega F_{\tau,x} F_s \, d\Omega \int_l N_i N_{j,y} \, dy + \\ & \widetilde{C}_{13} \int_\Omega F_\tau F_{s,z} \, d\Omega \int_l N_{i,y} N_j \, dy + \widetilde{C}_{36} \int_\Omega F_\tau F_{s,x} \, d\Omega \int_l N_{i,y} N_j \, dy \end{aligned} \tag{18}$$

The comprehensive set of nine components of *fundamental nucleus* are addressed in Appendix. It should be noted that no assumptions on the expansion order have been done. Therefore, it is possible to obtain refined beam models without changing the formal expression of the nucleus components. In fact, it has the property to be invariant with respect to the theory order and the element type. Shear locking is corrected through selective integration.[31]

As far as the nodal load vector is concerned, it is obtained by writing the virtual work of external loads δL_{ext}. The nodal load vector variationally coherent to the above method is derived here for the case of a generic concentrated load $\boldsymbol{P}$ acting on the load application point $\left(x_P, y_P, z_P \right)$:

$$\boldsymbol{P} = \left\{ P_{u_x} \quad P_{u_y} \quad P_{u_z} \right\}^T \tag{19}$$

At first, the virtual work due to P involves the virtual variation of the displacement vector:

$$\delta L_{ext} = \delta \boldsymbol{u}^T \boldsymbol{P} \tag{20}$$

Finally, by substituting Eq. 13, δL_{ext} can be written involving the virtual variation of nodal displacements:

$$\delta L_{ext} = \delta \boldsymbol{q}_{\tau i}^T F_\tau N_i \boldsymbol{P} \tag{21}$$

where F_τ is evaluated in (x_P, z_P) and N_i is calculated in y_P. Any other loading condition can be similarly treated.

V.   Aeroelastic notation

The invariance and the increasing accuracy of the model as the expansion order increases allows to study beam-like structures, where one dimension is predominant but not insomuch as to rigorously account them as beams. It means that the model is able to evaluate the structural behavior also of wing systems. That is the reason why it is possible to extend the formulation to the *aeroelastic analysis* of non-planar wing configurations.

A global coordinate system $x-y-z$ is placed on the leading edge point of the root wing section airfoil (see Fig. 4). The global x axis is parallel to the free stream velocity $\boldsymbol{V}_\infty$ and directed toward the trailing edge, assuming the yaw angle of the aircraft equal to zero. Whereas, the global y axis goes along the spanwise

direction toward the tip of the right half-wing.

Considering a wing system generally oriented in the 3D space, the method allows to divide it into a set of large trapezoidal wing segments, according to the same logic used in other previous aeroelastic works (see Demasi and Livne[32]). The number of these trapezia is denoted as N_{WS}. As we will see later, the wing system will be divided into aerodynamic panels. In the present formulation they are located on the aerodynamic reference surfaces of the wing system with initial angle of attack equal to zero. Thanks to the possibility of studying non-planar configuration, each wing segment can have dihedral or sweep angle. Moreover, it is assumed that all the wing segments have two opposite segments parallel to the wind direction, i.e. parallel to the global x axis.

Each wing segment contains a local coordinate system $x^S - y^S - z^S$, where S is the superscript for the generic wing segment. As shown in Fig. 2, the wing segment itself lies in the plane $x^S - y^S$. In particular, the x^S axis has to be always parallel to the free stream $\boldsymbol{V}_\infty$. As a consequence, x^S is parallel to global x axis for each wing segment. The y^S axis is not parallel to y only if the wing segment has a dihedral different from zero. The origin of the local coordinate system is placed on one of the two leading edges of the wing segment. The point is located so that the other one has a positive value of local y^S coordinate.
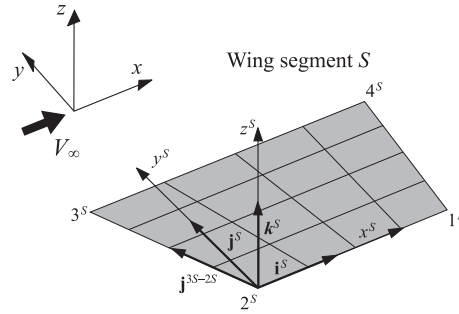

Figure 2. Local coordinate system and numbering convention for a Wing Segment.

The aerodynamic method here chosen is the Vortex Lattice Method[38] (VLM). The structure is subdivided into a lattice of quadrilateral aerodynamic panels. A horseshoe element is placed on each panel. This element consists of a straight bound vortex BC and two semi-infinite trailing vortex lines AB and CD. Here, the bound vortex is placed at the panel's quarter chord line and the load point P_L is in the middle of such a bound vortex. Whereas, the control point P_C (also called collocation point) is located at the center of the panel's three-quarter chord line.[38] The typical horseshoe scheme is shown in Fig. 3.
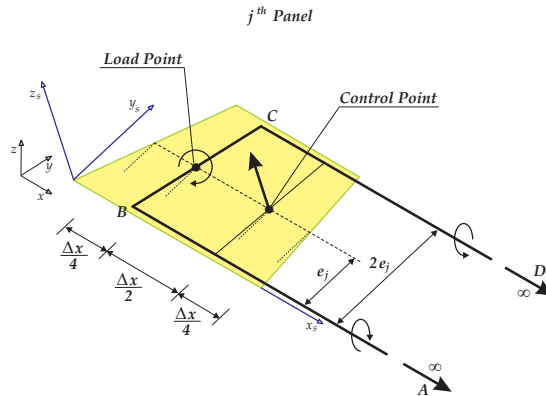

Figure 3. The horseshoe convention followed for the VLM.

Since the structure has been subdivided into a set of wing segments, the aerodynamic mesh lies on these reference surfaces, which are assumed to have an angle of attack equal to zero. That does not mean that the incidence of the wing system is not considered in the model, but just that it is not faced in the discretization. In fact, the angle of attack of the structure will be used in the construction of a term denoted as $\boldsymbol{L}_{RHS}$. However, it must not be very large, in order to have a problem case where the linear aerodynamic analysis

remains a valid approximation.

For each wing segment it is assigned a straight beam perpendicular to the global x axis and contained in the plane $x^S - y^S$, over which the 1D structural refined elements mesh is created. Each beam element must be entirely contained in a plane orthogonal to the global x axis (wind direction). All the elements constituting the whole structural mesh are connected. For instance, Fig. 4 shows the application of the method to a typical C-Wing configuration, which is divided into differently coloured wing segments.
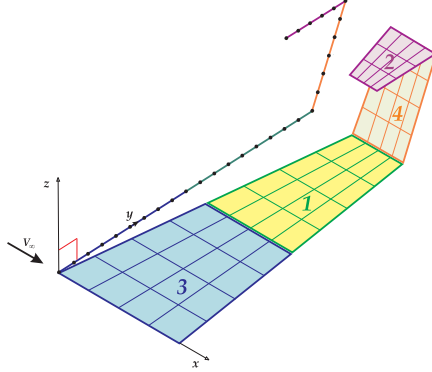

Figure 4. Unidimensional structural mesh and bidimensional aerodynamic mesh of wing segments.

It should be noted that the origin of the coordinate system on the cross-section of a generic finite element does not necessarily coincide with the centroid of the section itself. Moreover, such an origin in general can be located outside the cross-section area, as shown in Fig. 1.

To summarize, the model studies the deformation of a wing system generally oriented in the 3D space by means of refined finite elements in general not lying on the wing surface.

VI.   Aeroelastic formulation

At first, the above mentioned structural formulation has to be extended in order to study *generally oriented* beam-like structures. In fact, the fundamental nuclei have been obtained in the local coordinate system of the element. Considering the generic wing segment S, Eq. 17 written in its local coordinate system becomes:

$$\delta L_i \,=\, \delta \boldsymbol{q}^{S\,T}_{\tau i\,\text{loc}} \;\; \boldsymbol{K}^{ij\tau s\,S}_{\text{loc}} \; \boldsymbol{q}^{S}_{sj\,\text{loc}} \tag{22}$$

This expression is in general valid in *local coordinate system*, whose y^S axis is parallel to the element beam axis. For the general purpose of this work, it is necessary to extend the formulation to the global coordinate system. The problem consists in a typical transformation of coordinates by means of orthogonal matrices. Let $\boldsymbol{i}^S$, $\boldsymbol{j}^S$ and $\boldsymbol{k}^S$ be the unit vectors of the local coordinate system. They are expressed in global coordinates via the corresponding unit vectors $\boldsymbol{i}$, $\boldsymbol{j}$ and $\boldsymbol{k}$ (see Fig. 2):

$$\begin{aligned}
\boldsymbol{i}^S &= e^S_{11}\,\boldsymbol{i} \,+\, e^S_{12}\,\boldsymbol{j} \,+\, e^S_{13}\,\boldsymbol{k} \\
\boldsymbol{j}^S &= e^S_{21}\,\boldsymbol{i} \,+\, e^S_{22}\,\boldsymbol{j} \,+\, e^S_{23}\,\boldsymbol{k} \\
\boldsymbol{k}^S &= e^S_{31}\,\boldsymbol{i} \,+\, e^S_{32}\,\boldsymbol{j} \,+\, e^S_{33}\,\boldsymbol{k}
\end{aligned} \tag{23}$$

where the 9 coefficients are the global coordinates of local unit vectors. By isolating such terms in a matrix 3×3, any vector of local nodal displacements can be expressed in global coordinates as follows:

$$\boldsymbol{q}^S_{sj\,\text{loc}} \,=\, \boldsymbol{e}^S \,\cdot\, \boldsymbol{q}^S_{sj} \tag{24}$$

The substitution of Eq. 24 in Eq. 22 leads to write the fundamental nucleus of Structural Stiffness Matrix in the global coordinate system:

$$\delta L_i \,=\, \delta \boldsymbol{q}^{S\,T}_{\tau i\,\text{loc}} \;\; \boldsymbol{K}^{ij\tau s\,S}_{\text{loc}} \; \boldsymbol{q}^{S}_{sj\,\text{loc}} \,=\, \delta \boldsymbol{q}^{S\,T}_{\tau i} \left[\boldsymbol{e}^{S\,T} \cdot \boldsymbol{K}^{ij\tau s\,S}_{\text{loc}} \cdot \boldsymbol{e}^S \right] \boldsymbol{q}^{S}_{sj} \tag{25}$$

American Institute of Aeronautics and Astronautics

Before the assembly procedure the FE structural matrices must be rotated to impose the compatibility of the displacements expressed in global coordinates:

$$\boldsymbol{K}^{ij\tau s\,S} = \left[\boldsymbol{e}^{S\,T} \cdot \boldsymbol{K}^{ij\tau s\,S}_{\mathrm{loc}} \cdot \boldsymbol{e}^{S} \right] \tag{26}$$

The assembly procedure on beam elements of different wing segments will be performed in the classical way, summing up the stiffness terms corresponding to the common nodes.

A. Splining and Pseudo-Structural Points

The coupling of structural and aerodynamic fields is carried out by a splining method. Although the present Finite Element Model is unidimensional, the splining is not performed by means of the Beam Spline method,[33−34] but indeed of the Infinite Plate Spline method[35−37] (IPS). The reason is due to the accuracy of refined element in predicting displacements of points not necessarily coincident with the actual FEM nodes and not even located on the element axis.

On the reference plane of each Wing Segment (the generic one is indicated with superscript S) a set of N^S_{PS} aeroelastic points is chosen and the corresponding displacements are computed by the structural formulation. Then, these deflections will be utilized as input data in order to mathematically describe the deformed surface of wing segment S via IPS method. The points forming the set are denoted as *pseudo-structural points*, precisely because they has the meaning of structural points (the spline surface is treated as a plate by IPS method). The adjective *pseudo* is adopted to not confuse them with structural nodes of the beam elements.

Defining the vector $\boldsymbol{x}$ as the vector which contains the global coordinates of pseudo-structural points of the entire wing system, it is possible to extract the global coordinates of the pseudo-structural points located on wing segment S and define the vector $\boldsymbol{x}^S$ by means of matrix $\boldsymbol{J}^S$. Since the point 2^S is the origin of the local coordinate system of wing segment S (see Fig. 2), the vector $\boldsymbol{x}_{2^s}$ (with dimension $3N^S_{PS} \times 1$) is introduced:

$$\boldsymbol{x}_{2^s} = \left\{ x_{2^s} \quad y_{2^s} \quad z_{2^s} \quad ... \quad x_{2^s} \quad y_{2^s} \quad z_{2^s} \right\}^T \tag{27}$$

The coordinates $\boldsymbol{x}^S_{\mathrm{loc}}$ of the pseudo-structural points lying on wing segment S expressed in the local reference system are determined by defining the block diagonal matrix $\boldsymbol{E}^S$, where the transformation matrix $\boldsymbol{e}^S$ is repeated as many times as N^S_{PS}:

$$\boldsymbol{x}^S_{\mathrm{loc}} = \boldsymbol{E}^S \cdot \left\{ \boldsymbol{x}^S - \boldsymbol{x}_{2^s} \right\} = \boldsymbol{E}^S \cdot \left\{ \boldsymbol{J}^S \cdot \boldsymbol{x} - \boldsymbol{x}_{2^s} \right\} \tag{28}$$

Remembering that $\boldsymbol{q}$ is the vector of the nodal degrees of freedom (in global coordinate system) of all nodes on the beams, it is possible to extract the vector $\boldsymbol{q}^S$ of nodal displacements (in global coordinate system) corresponding to wing segment S only, by means of matrix $\boldsymbol{I}^S$.

It is now possible to convert the vector $\boldsymbol{q}^S$ in *local* coordinates using a formula similar to Eq. 24, by introducing the matrix $\boldsymbol{E}^S_q$. It is a block diagonal matrix containing the transformation matrix $\boldsymbol{e}^S$ for each degree of freedom of the structural nodes corresponding to wing segment S. Therefore:

$$\boldsymbol{q}^S_{\mathrm{loc}} = \boldsymbol{E}^S_q \cdot \boldsymbol{q}^S = \boldsymbol{E}^S_q \cdot \boldsymbol{I}^S \cdot \boldsymbol{q} \tag{29}$$

To utilize the Finite Element formulation, it is mandatory to individualize the corresponding finite element for each pseudo-structural point. The parameter to be analyzed is the local y^S coordinate, which is extracted from vector $\boldsymbol{x}^S_{\mathrm{loc}}$. In fact, by using that value it is possible to "assign" that pseudo-structural point to a particular beam element on wing segment S. Everything is expressed in local coordinates and so the FEM equation 30 can be used to calculate the local displacements according to CUF:

$$\boldsymbol{u}^S_{\mathrm{loc}}\left(x^S, y^S, z^S\right) = F_\tau\left(x^S, z^S\right) \boldsymbol{u}^S_{\tau\,\mathrm{loc}}\left(y^S\right) = F_\tau\left(x^S, z^S\right) N_i\left(y^S\right) \boldsymbol{q}^S_{\mathrm{loc}} \tag{30}$$

The same expression can be repeated for all the pseudo-structural points of wing segment S, noting that each of them has zero angle of attack and so $z^S = 0$. Resuming Eq. 29, this means that for each wing segment it is possible to define a matrix $\boldsymbol{Y}^S$ which relates the vector of nodal degrees of freedom in local coordinates of wing segment S with the displacements $\tilde{\boldsymbol{u}}^S_{\mathrm{loc}}$ (in local coordinates) of all the pseudo-structural points. Then,

American Institute of Aeronautics and Astronautics

calling $\boldsymbol{I}_z^S$ the constant matrix which allows the extraction of z^S component of the local displacements it is possible to write Eq. 31:

$$\boldsymbol{Z}_{\text{loc}}^S \;=\; \boldsymbol{I}_z^S \,\cdot\, \tilde{\boldsymbol{u}}_{\text{loc}}^S \;=\; \boldsymbol{I}_z^S \,\cdot\, \boldsymbol{Y}^S \cdot\, \boldsymbol{q}_{\text{loc}}^S \;=\; \boldsymbol{I}_z^S \,\cdot\, \boldsymbol{Y}^S \cdot\, \boldsymbol{E}_q^S \,\cdot\, \boldsymbol{I}^S \cdot\, \boldsymbol{q} \tag{31}$$

The vector $\boldsymbol{Z}_{\text{loc}}^S$ in Eq. 31 contains the z^S coordinates of the *deformed* configuration and so the input data for the spline method. Using the fitted surface spline shape it is possible to calculate the derivatives of such a shape and the associated local angle of attack. The local z coordinate of the pseudo-structural point i on wing segment S is:

$$Z_{i\,\text{loc}}^S \;=\; Z_{i\,\text{loc}}^S \left(x_{i\,\text{loc}}^S,\, y_{i\,\text{loc}}^S \right) \tag{32}$$

The *assumption* that the displacements are not very large is made. In fact, a linear theory is utilized, then it is appropriate to assume small displacements. So, the aerodynamic linear theory holds. Under this assumption, it is reasonable to consider the local in-plane coordinates of the nodes, the load and control points of a generic wing segment constant. Only the out-of-plane local displacement will be different from zero. Under this hypothesis, all the splining matrices are constant and they can be calculated once.

According to the IPS method, for each pseudo-structural point i of wing segment S the corresponding $Z_{i\,\text{loc}}^S$ is written as:

$$Z_{i\,\text{loc}}^S \left(x_{i\,\text{loc}}^S,\, y_{i\,\text{loc}}^S \right) \;=\; a_0^S \;+\; a_1^S\, x_{i\,\text{loc}}^S \;+\; a_2\, y_{i\,\text{loc}}^S \;+\; \sum_{j=1}^{N_{PS}^S} F_j\, K_{ij}^S \left(r_{ij\,\text{loc}}^S \right)^2 \ln\!\left(r_{ij\,\text{loc}}^S \right)^2 \tag{33}$$

where:

$$K_{ij}^S \;=\; \left(r_{ij\,\text{loc}}^S \right)^2 \ln\!\left(r_{ij\,\text{loc}}^S \right)^2 \tag{34}$$

$$\left(r_{ij\,\text{loc}}^S \right)^2 \;=\; \left(x_{i\,\text{loc}}^S - x_{j\,\text{loc}}^S \right)^2 \;+\; \left(y_{i\,\text{loc}}^S - y_{j\,\text{loc}}^S \right)^2 \tag{35}$$

noting that also the counter j refers to pseudo-structural points. For the sake of brevity, the details about the IPS method[35−37] are not reported here. Writing Eq. 33 for all the pseudo-structural points and combining the infinite conditions, the following matrix notation is obtained:

$$\boldsymbol{Z}_{\text{loc}}^{S\star} \;=\; \begin{bmatrix} \boldsymbol{0} & \boldsymbol{R}^S \\[4pt] \left[\boldsymbol{R}^S \right]^T & \boldsymbol{K}^S \end{bmatrix} \cdot\, \boldsymbol{P}^S \;=\; \boldsymbol{G}^S \cdot\, \boldsymbol{P}^S \tag{36}$$

By inverting Eq. 36, it is possible to find the $N_{PS}^S + 3$ unknowns represented by the spline coefficients $\boldsymbol{P}^S$.

Once obtained the coefficients necessary to describe the spline, then the aerodynamic points of the panels are taken into account. To impose the boundary conditions the derivatives with respect to x^S are required at control points. Therefore, it is necessary to differentiate the spline equation 33 with respect to x^S and calculate the result in the local coordinates of control points. Let $\left(\mathcal{X}_{k\,\text{loc}}^S,\, \mathcal{Y}_{k\,\text{loc}}^S \right)$ be the local coordinates (in the reference plane) of the kth control point. Its slope is given by:

$$\frac{\mathrm{d}\mathcal{Z}_{k\,\text{loc}}^S}{\mathrm{d}x^S} \left(\mathcal{X}_{k\,\text{loc}}^S,\, \mathcal{Y}_{k\,\text{loc}}^S \right) = a_1 + \sum_{j=1}^{N_{PS}^S} F_j\, \mathcal{D}_{kj}^S = a_1 + \sum_{j=1}^{N_{PS}^S} F_j \left[2\left(\mathcal{X}_{k\,\text{loc}}^S - x_{j\,\text{loc}}^S \right) \left[1 + \ln\!\left(\mathcal{R}_{kj\,\text{loc}}^S \right)^2 \right] \right] \tag{37}$$

where:

$$\left(\mathcal{R}_{kj\,\text{loc}}^S \right)^2 \;=\; \left(\mathcal{X}_{k\,\text{loc}}^S - x_{j\,\text{loc}}^S \right)^2 \;+\; \left(\mathcal{Y}_{k\,\text{loc}}^S - y_{j\,\text{loc}}^S \right)^2 \tag{38}$$

Following the exposed procedure for all the N_{AP}^S (= Number of Aerodynamic Panels of wing segment S) locations on the surface, the slopes can be written as functions of the spline coefficients in a compact form:

$$\frac{\mathrm{d}\boldsymbol{\mathcal{Z}}_{\text{loc}}^S}{\mathrm{d}x^S} \;=\; \boldsymbol{\mathcal{D}}^S \cdot\, \boldsymbol{P}^S \tag{39}$$

Now, it is advantageous to write an expression able to relate directly the output and the input data, represented by the z^S coordinates of pseudo-structural points in the deformed configuration:

$$\frac{\mathrm{d}\boldsymbol{\mathcal{Z}}_{\text{loc}}^S}{\mathrm{d}x^S} \;=\; \boldsymbol{\mathcal{D}}^S \cdot\, \boldsymbol{P}^S \;=\; \boldsymbol{\mathcal{D}}^S \cdot\, \left[\boldsymbol{G}^S \right]^{-1} \cdot\, \boldsymbol{Z}_{\text{loc}}^{S\star} \;=\; \boldsymbol{\mathcal{D}}^S \cdot\, \boldsymbol{S}^S \cdot\, \boldsymbol{Z}_{\text{loc}}^S \tag{40}$$

where $\boldsymbol{S}^S$ is the matrix $\left[\boldsymbol{G}^S\right]^{-1}$ with the first three columns eliminated, without changing the result. Combining Eqs. 31 and 40, the following expression relates the slope of control points of all the panels in wing segment S to the vector of nodal degrees of freedom of the whole structure:

$$\frac{\mathrm{d}\boldsymbol{\mathcal{Z}}_{\mathrm{loc}}^S}{\mathrm{d}x^S} = \boldsymbol{\mathcal{D}}^S \cdot \boldsymbol{S}^S \cdot \boldsymbol{I}_z^S \cdot \boldsymbol{Y}^S \cdot \boldsymbol{E}_q^S \cdot \boldsymbol{I}^S \cdot \boldsymbol{q} = \boldsymbol{\mathcal{D}}^S \, \boldsymbol{a}_3^S \cdot \boldsymbol{q} \tag{41}$$

Equation 41 can be written for all wing segments and so an *assembly procedure* is required to have all the local slopes of all the panels of the entire wing system as a function of degrees of freedom of all the structural finite elements.

While calculating the generalized aerodynamic matrices, it is required to transform lift forces at aerodynamic load points into nodal forces on the structural grid nodes. This transformation will involve the displacements of load points. The matrix relating the input displacements at pseudo-structural points to the output deflections at load points is addressed as $\widetilde{\boldsymbol{\mathcal{D}}}^{S\star}$ and built following the spline equation 33. The procedure needs the local coordinates of load points $\widetilde{\mathcal{Y}}_{I\,\mathrm{loc}}^S$. Finally, the displacement vector at load points can be written as function of the nodal degrees of freedom by using a procedure formally identical to the one used to obtain Eq. 41:

$$\widetilde{\boldsymbol{\mathcal{Z}}}_{\mathrm{loc}}^S = \widetilde{\boldsymbol{\mathcal{D}}}^{S\star} \cdot \boldsymbol{P}^S = \widetilde{\boldsymbol{\mathcal{D}}}^{S\star} \cdot \boldsymbol{S}^S \cdot \boldsymbol{I}_z^S \cdot \boldsymbol{Y}^S \cdot \boldsymbol{E}_q^S \cdot \boldsymbol{I}^S \cdot \boldsymbol{q} = \widetilde{\boldsymbol{\mathcal{D}}}^{S\star} \, \boldsymbol{a}_3^S \cdot \boldsymbol{q} \tag{42}$$

The assembly process is carried out by calculating all the products (for all wing segments) $\boldsymbol{\mathcal{D}}^S \, \boldsymbol{a}_3^S$ and $\widetilde{\boldsymbol{\mathcal{D}}}^{S\star} \, \boldsymbol{a}_3^S$ and observing that each aerodynamic panel can be included only in one trapezoidal wing segment. In fact, different wing segments don't share common aerodynamic panels. After the assembly, Eqs. 41 and 42 written at wing system level become:

$$\frac{\mathrm{d}\boldsymbol{\mathcal{Z}}_{\mathrm{loc}}}{\mathrm{d}x} = \boldsymbol{A}_3 \cdot \boldsymbol{q} \tag{43}$$

$$\widetilde{\boldsymbol{\mathcal{Z}}}_{\mathrm{loc}} = \widetilde{\boldsymbol{A}}_3^{\star} \cdot \boldsymbol{q} \tag{44}$$

By means of the exposed matricial notation, Eqs. 43 and 44 allow to directly relate displacements and slopes at aerodynamic points of the structure to its nodal degrees of freedom.

B. Steady Aerodynamic Forces

Now the derivation of aerodynamic loads is faced. According to the Vortex Lattice Method,[38] the pressures acting on the deflecting surface are transferred as lift forces located on loads points of the aerodynamic panels of the whole structure. Considering the generic j^{th} panel of wing segment S and dimensionless pressure acting on it, the modulus of the lift force applied at the corresponding load point is given by:

$$\left|L_j^S\right| = \frac{1}{2}\,\rho_\infty\,V_\infty^2\,\Delta x_j\,2e_j\,\Delta p_j^S \tag{45}$$

where the quantity Δx_j is the average chord of the panel and e_j refers to its half-length along y^S local axis (wing spanwise direction). Since the reference aerodynamic configuration has no angle of attack, it should be noted that lift forces are normal to the panels and perpendicular to the wind direction. Let $\Delta\boldsymbol{p}$ be the vector containing the dimensionless pressure loads acting on all the aerodynamic panels of the structure, normalized with respect to the dynamic pressure. The lift forces moduli are written in a matrix form:

$$\boldsymbol{L} = \frac{1}{2}\,\rho_\infty\,V_\infty^2\,\boldsymbol{I}^D \cdot \Delta\boldsymbol{p} \tag{46}$$

where $\boldsymbol{I}_D$ contains the panels' geometrical data. The VLM allows to describe the dimensionless normalwash, normalized with respect to V_∞, as function of the pressures acting on each aerodynamic panel:

$$\boldsymbol{w} = \boldsymbol{A}^D \cdot \Delta\boldsymbol{p} \tag{47}$$

where $\boldsymbol{A}^D$ is the Aerodynamic Influence Coefficient Matrix. It is calculated by using the geometrical data of the aerodynamic mesh. In the steady case, considering that the structure changes configuration when it deforms, the *boundary condition* used for the Vortex Lattice formulation is:

$$\boldsymbol{w} = \frac{\mathrm{d}\boldsymbol{\mathcal{Z}}_{\mathrm{loc}}}{\mathrm{d}x} \tag{48}$$

Considering small angles of deflection because of the model's linearity, Eq. 48 means that the dimensionless normalwash has to equal the slope at the aerodynamic control point. The boundary condition is not only a constraint expressing the coupling between aerodynamics and deflection of the structure, but in this case it is the interface able to correlate the lifting surface to the nodal degrees of freedom. As a result, by combining Eqs. 43 and 46 - 48, the vector containing the aerodynamic forces is written as function of nodal degrees of freedom:

$$\boldsymbol{L} \; = \; \frac{1}{2}\,\rho_\infty\,V_\infty^2\,\boldsymbol{I}^D \cdot \left[\boldsymbol{A}^D\right]^{-1} \cdot \boldsymbol{w} \; = \; \frac{1}{2}\,\rho_\infty\,V_\infty^2\,\boldsymbol{I}^D \cdot \left[\boldsymbol{A}^D\right]^{-1} \cdot \boldsymbol{A}_3 \cdot \boldsymbol{q} \; = \; \frac{1}{2}\,\rho_\infty\,V_\infty^2\,\overline{\boldsymbol{c}} \cdot \boldsymbol{q} \qquad (49)$$

where the matrix $\overline{\boldsymbol{c}}$ has been conveniently introduced.

C. The Aeroelastic Stiffness Matrix

The aerodynamic forces of Eq. 49 are applied at load points of the aerodynamic panels. They are transferred to the structural nodes using the following algorithm. The result will be a vector of equivalent nodal loads, by means of which the construction of the Aeroelastic Stiffness Matrix will be carry out. From Eq. 49 it is possible to extract the forces applied only on panels of the generic wing segment S:

$$\boldsymbol{L}^S \; = \; \frac{1}{2}\,\rho_\infty\,V_\infty^2\,\overline{\boldsymbol{c}}^S \cdot \boldsymbol{q} \qquad (50)$$

where $\overline{\boldsymbol{c}}^S$ is directly obtained from $\overline{\boldsymbol{c}}$. The lift forces are parallel and perpendicular to the surface representing the wing segment S, then local x^S, y^S components of the aerodynamic loads are zero. Hence, $\boldsymbol{L}^S$ contains not only the moduli of the loads on aerodynamic panels of wing segment S, but also their local z^S components.

The transfer from loads at the aerodynamic points to the *energetically* equivalent loads at structural nodes is performed via the Principle of Virtual Displacements. Resuming Eq. 42, the balance between the virtual work carried out by lift forces on the virtual variation of displacements of load points and the virtual work carried out by equivalent nodal forces on the virtual variation of nodal degrees of freedom is written as:

$$\delta W \; = \; \left\{\delta\widetilde{\boldsymbol{\mathcal{Z}}}_{\text{loc}}^S\right\}^T \cdot \boldsymbol{L}^S \; = \; \left\{\widetilde{\boldsymbol{\mathcal{D}}}^{S\star}\boldsymbol{a}_3^S \cdot \delta\boldsymbol{q}\right\}^T \cdot \boldsymbol{L}^S \; = \; \delta\boldsymbol{q}^T \cdot \left[\boldsymbol{a}_3^S\right]^T \cdot \left[\widetilde{\boldsymbol{\mathcal{D}}}^{S\star}\right]^T \cdot \boldsymbol{L}^S \; = \; \delta\boldsymbol{q}^T \cdot \boldsymbol{L}_{\text{str}}^S \qquad (51)$$

where the virtual variation of nodal degrees of freedom $\boldsymbol{q}$ is considered. The vector $\boldsymbol{L}_{\text{str}}^S$ contains the nodal forces on all structural nodes. The superscript S indicates that only the aerodynamic loads applied at the panels of wing segment S have been taken into account. Combining Eqs. 51 and 50 it is possible to deduce:

$$\boldsymbol{L}_{\text{str}}^S \; = \; \left[\boldsymbol{a}_3^S\right]^T \cdot \left[\widetilde{\boldsymbol{\mathcal{D}}}^{S\star}\right]^T \cdot \boldsymbol{L}^S \; = \; \frac{1}{2}\,\rho_\infty\,V_\infty^2\,\left[\boldsymbol{a}_3^S\right]^T \cdot \left[\widetilde{\boldsymbol{\mathcal{D}}}^{S\star}\right]^T \cdot \overline{\boldsymbol{c}}^S \cdot \boldsymbol{q} \qquad (52)$$

If all the contributions of all wing segments are added following Eq. 52, the loads on the structural nodes can be obtained. This operation means that an *assembly* of the matrices $\frac{1}{2}\,\rho_\infty\,V_\infty^2\,\left[\boldsymbol{a}_3^S\right]^T \cdot \left[\widetilde{\boldsymbol{\mathcal{D}}}^{S\star}\right]^T \cdot \overline{\boldsymbol{c}}^S$ is required. The final assembled matrix is named $-\,\boldsymbol{K}_{\text{aero}}$, where the negative sign is adopted for the sake of convenience. The expression of aerodynamic loads on all the structural nodes after all wing segments have been taken into account is:

$$\boldsymbol{L}_{\text{str}} \; = \; -\,\boldsymbol{K}_{\text{aero}} \cdot \boldsymbol{q} \qquad (53)$$

Such a term can go to the left hand side of the aeroelastic equation system and summed up to the product due to the Structural Stiffness:

$$\boldsymbol{K}_{\text{str}} \cdot \boldsymbol{q} \; = \; \boldsymbol{L}_{\text{str}} \; = \; -\,\boldsymbol{K}_{\text{aero}} \cdot \boldsymbol{q} \qquad (54)$$

or

$$\left[\boldsymbol{K}_{\text{str}} \; + \; \boldsymbol{K}_{\text{aero}}\right] \cdot \boldsymbol{q} \; = \; \boldsymbol{0} \qquad (55)$$

or

$$\boldsymbol{K}_{\text{aeroelastic}} \cdot \boldsymbol{q} \; = \; \boldsymbol{0} \qquad (56)$$

The isolation of the stiffness matrices in Eq. 55 leads to a unique term, called *Aeroelastic Stiffness Matrix*. Practically, it substitutes the Structural Stiffness Matrix in the FEM system, so that the stiffness of the

American Institute of Aeronautics and Astronautics

structure is sensible to and inclusive of the aerodynamic loads applied. In this way the deflection due to such loads is already taken into account directly in the stiffness of the system.

From Eq. 56 it appears that there is no motion. It occurs because the angle of attack so far considered is zero. So, there is no motion unless we have external non-aerodynamic loads, i.e. some mechanical loads. To solve this problem, a given known shape of the structure is assigned, for instance, by points having local coordinates x^S and y^S of pseudo-structural points. Whereas, the z^S local out-of-plane coordinates are not equal to zero and describe a shape with *different from zero angle of attack*. The new points will be denoted as perturbed pseudo-structural points. The corresponding aerodynamic loads are computed as concentrated forces localized on the load points and are transformed as energetically equivalent loads at the structural nodes. Following the same procedure used to find the Aeroelastic Stiffness Matrix, the loads $\boldsymbol{L}_{\text{RHS}}$ on the structural nodes can be obtained (the subscript RHS means Right Hand Side). At the end, the final aeroelastic equation to be solved is:

$$\left[\boldsymbol{K}_{\text{str}} \, + \, \boldsymbol{K}_{\text{aero}} \right] \, \cdot \, \boldsymbol{q} \, = \, \boldsymbol{L}_{\text{RHS}} \tag{57}$$

or

$$\boldsymbol{K}_{\text{aeroelastic}} \, \cdot \, \boldsymbol{q} \, = \, \boldsymbol{L}_{\text{RHS}} \tag{58}$$

Equation 58 allows to compute the vector of unknowns nodal degrees of freedom $\boldsymbol{q}$. Now that the right hand side is different from zero, we have a solution.

VII.   Results

The structural and aeroelastic results are presented here. The analyses have been executed on a series of different geometrical configurations. The beam's cross-sections analyzed in this work are rectangular or square and clamped boundary condition is accounted for. An isotropic material is used. The Young's modulus E is equal to $69\,[GPa]$ and the Poisson's ratio ν is equal to 0.33. For the exposed results a selective integration of the shape functions along the beam axis is adopted.

The structural assessment of the refined finite element is carried out in order to validate its propriety in comparison with some classical analytical results and NASTRAN simulations. Beams subjected to bending and torsional loadings are analyzed. As far as the aeroelastic assessment is concerned, some aeroelastic analyses have been performed on planar and non-planar wing configurations. The corresponding results have been validated with NASTRAN.

A.   Structural Assessment

For the first structural assessment, the beam's rectangular cross-section has dimension $3 \times 60\,[mm]$, whereas the length L is equal to $600\,[mm]$. For example, the beam could simulate the wind tunnel model for a glider wing. The loading condition is a pure bending about the local x^S axis. The concentrated bending load P_{u_z} (equal to $1\,N$) acts on the centroid of the tip cross-section. The mechanics of the beam is described in terms of dimensionless maximum vertical displacement, $\bar{u}_{z\,\text{max}}$, which is computed at the center point of the tip cross-section. Such a dimensionless displacement is normalized with respect to the following value given by the Euler-Bernoulli beam theory, which is taken as reference solution:

$$u^{\star}_{z\,\text{max}} \, = \, \frac{P_{u_z}\,L^3}{3\,E\,I} \, = \, 7.7295\,mm \qquad \bar{u}^{\star}_{z\,\text{max}} \, = \, 1.0000 \tag{59}$$

where I is the moment of inertia of the beam cross-section. A structural convergence study is carried out to evaluate the effect of the number of Finite Elements N_{EL} constituting the structural mesh on results. Then, a further structural convergence study on the effect of the expansion order N defining the Unified Formulation is performed. Such convergence analyses are conducted for the three elements B4, B3, B2, with 4, 3, 2 nodes respectively. Their results are shown in Tables 2 - 4.

According to the typical behavior of FEM solutions, the maximum tip displacement increases and becomes more accurate as N_{EL} increases. An excellent correspondence is obtained between the refined model's and NASTRAN results, which are slightly different from the approximated Euler-Bernoulli solution of Eq. 59. When the expansion order is $N = 4$, Fig. 5 describes the behavior of the solution when the number of elements (B2, B3 and B4) increases and proves graphically such a correspondence. The results and the

American Institute of Aeronautics and Astronautics

accuracy of the structural model change as N changes. Anyway, after $N = 3$ the final result appears not to be evidently variable and then the convergence on N is reached. Finally, the deflection along the beam axis is investigated in Fig. 6.

As second load case, the cantilever beam is subjected to a torsional loading located on the tip cross-section. The previous beam has been replaced with a square cross-section beam, but keeping the same lenght. It results to be slender with a high span-to-height ratio. The load is reproduced by two opposite concentrated forces acting on two points of the tip cross-section symmetrical with respect to the vertical z axis.

The investigation about the effect of expansion order N on the deflection of tip cross-section is summarized in Fig. 7. The first-order theory predicts the planarity of the cross-section in the deformed configuration. Second and third-order models yield similar results, with the deformation no more planar. Finally, the fourth-order clearly shows the warping effect on the tip cross-section. Hence, the deformed section has not a planar behavior, differently from the first-order theory and classical models. It has been demonstrated that the refined model for higher-order expansion is able to study beam-like structures more accurately than the classical models, highlighting the out-of-plane displacements of beam cross-sections. Then, the Unified Formulation provides an approximation of the tridimensional structural behavior in spite of the unidimensional discretization.

B.   Aroleastic Assessment

The aeroelastic assessment has the goal to validate the aeroelastic model by comparison with NASTRAN solutions (SOL 144). It is performed a convergence study similar to the analyses carried out for the structural assessment. Now, such a study evaluates the correctness of the interaction between structures and aerodynamics. For this purpose, the convergence on the number of aerodynamic VLM panels N_{AP} used to discretize the reference surfaces of wing segments is also investigated.

Here, the cases considered consist in three different wing configurations. The static aeroelastic responses of an unswept wing, a straight wing with dihedral and a swept tapered wing are investigated. In fact, the present beam formulation would be able to analyse a number of non-planar combinations of swept, tapered, dihedral wing segments. By exploiting the powerful of the method, the problem is solved by using right half-wing of each system only. Therefore, the aerodynamic computation takes into account the symmetry condition. The cross-section is always rectangular with thickness equal to 3 $[mm]$. For first two cases the chord is constant and equal to 60 $[mm]$, whereas the root and tip chords for the tapered wing are 100 $[mm]$ and 40 $[mm]$ respectively (see Fig. 8). The wingspan b does not change for the three cases and is equal to 1200 $[mm]$. The dihedral angle Γ used in case 2 is equal to 20 $[deg]$.

For the previous assessment the input loads were only mechanical and not aerodynamic. Now, the situation is opposite, since the only input load consists in the fact that the wing system is exposed to the free stream. Its velocity is equal to 40 $[m/s]$ and the considered air density is equal to 1.225 $[kg/m^3]$. The angle of attack for all the treated cases is equal to 1 $[deg]$. Again the mechanics of the beam is described in terms of the maximum vertical displacement, $u_{z\,max}$, which now is computed on the leading edge of the tip section. The analyses have been carried out by using the more accurate B4 element and its convergence for each aeroelastic case is reported on Tables 5, 7 and 9. Also for these aeroelastic problems, the maximum tip displacement increases for higher-order theories and becomes more accurated as N_{EL} increases. It is to note how the swept tapered requires a slightly greater number of elements to reach convergence, due to its particular geometry.

For the investigated cases, Tables 6, 8 and 10 summarize the values of static aeroelastic deflections as the number of aerodynamic VLM panels increases. Moreover, it is reported the trend as the expansion order N of the theory changes. The results are validated with commercial code NASTRAN (sol 144), which has performed aeroelastic analysis by coupling Doublet Lattice Method and structural shell elements. As expected, the solution approaches to more realistic values as the number of aerodynamic elements increases. Such a convergent trend occurs for all the shown theories, but well correspondence between the aeroelastic model's and NASTRAN results is obtained only when higher-order theories are involved. In particular, the typical torsional effect about y axis due to aerodynamic loadings is more accurately highlighted for large values of N. For swept tapered wings such an effect is presented in Fig. 11, whereas the tridimensional deflections of cases 1 and 3 are shown in Fig. 9 and 10.

Convergence study for Element B4

Load case: Bending $\qquad \bar{u}^{\star}_{z\,\mathrm{max}} = 1.0000 \qquad$ NASTRAN: 0.9880

N_{EL}	EBBM	TBM	$N = 1$	$N = 2$	$N = 3$	$N = 4$
2	0.9999	1.0000	1.0000	0.9344	0.9601	0.9604
5	1.0000	1.0000	1.0000	0.9486	0.9766	0.9776
10	1.0000	1.0000	1.0000	0.9532	0.9813	0.9826
20	1.0000	1.0000	1.0000	0.9555	0.9836	0.9850
40	1.0000	1.0000	1.0000	0.9567	0.9848	0.9862

Table 2. Structural case: Effect of the number of B4 elements on $\bar{u}_{z\,\mathrm{max}}$.

Convergence study for Element B3

Load case: Bending $\qquad \bar{u}^{\star}_{z\,\mathrm{max}} = 1.0000 \qquad$ NASTRAN: 0.9880

N_{EL}	EBBM	TBM	$N = 1$	$N = 2$	$N = 3$	$N = 4$
2	0.9999	1.0000	1.0000	0.9110	0.9307	0.9307
5	1.0000	1.0000	1.0000	0.9403	0.9669	0.9674
10	1.0000	1.0000	1.0000	0.9492	0.9772	0.9782
20	1.0000	1.0000	1.0000	0.9535	0.9816	0.9829
40	1.0000	1.0000	1.0000	0.9557	0.9838	0.9852

Table 3. Structural case: Effect of the number of B3 elements on $\bar{u}_{z\,\mathrm{max}}$.

Convergence study for Element B2

Load case: Bending $\qquad \bar{u}^{\star}_{z\,\mathrm{max}} = 1.0000 \qquad$ NASTRAN: 0.9880

N_{EL}	EBBM	TBM	$N = 1$	$N = 2$	$N = 3$	$N = 4$
2	0.9375	0.9375	0.9375	0.7907	0.7978	0.7978
5	0.9900	0.9900	0.9900	0.9035	0.9238	0.9240
10	0.9975	0.9975	0.9975	0.9332	0.9583	0.9589
20	0.9994	0.9994	0.9994	0.9462	0.9735	0.9745
40	0.9996	0.9999	0.9999	0.9522	0.9801	0.9813

Table 4. Structural case: Effect of the number of B2 elements on $\bar{u}_{z\,\mathrm{max}}$.
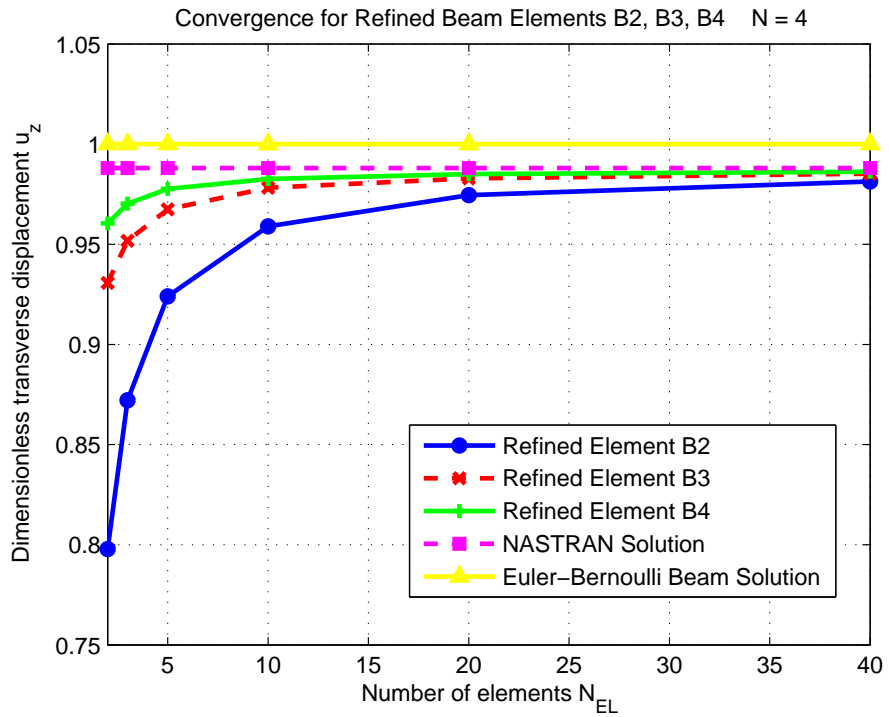
American Institute of Aeronautics and Astronautics
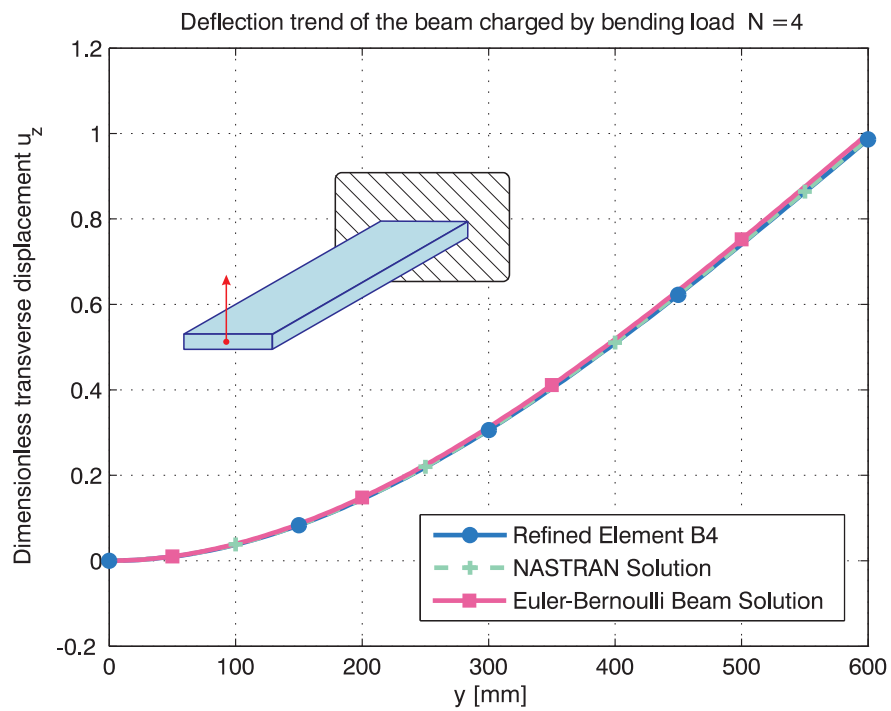
Figure 5. **Convergence study for Refined Elements.**

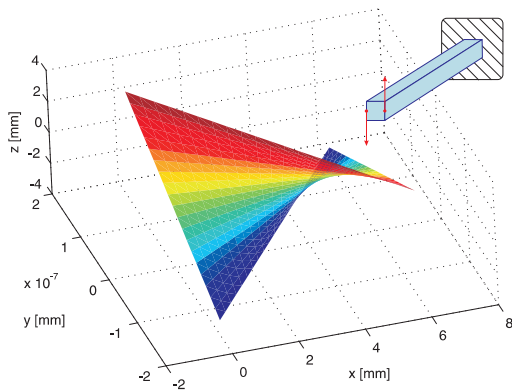Figure 6. **Deflection of the beam utilized for the convergence study.**
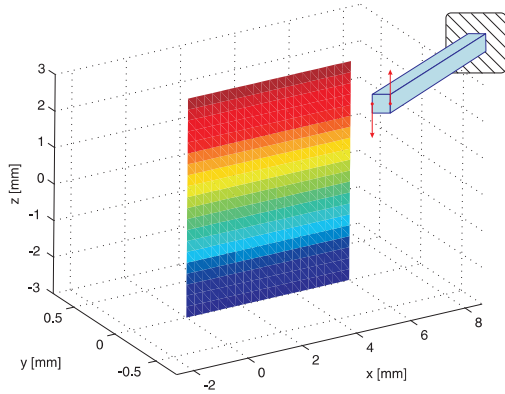
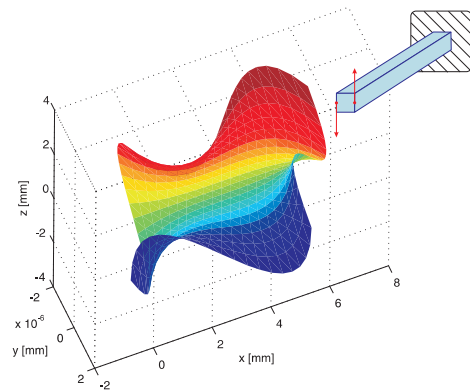American Institute of Aeronautics and Astronautics
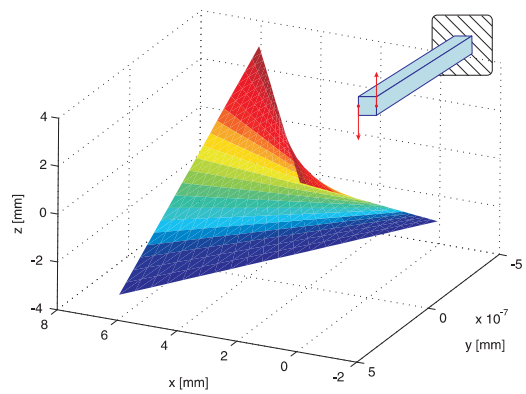
Figure 7. Deformed tip cross-section of the beam subjected to torsional load as N increases.
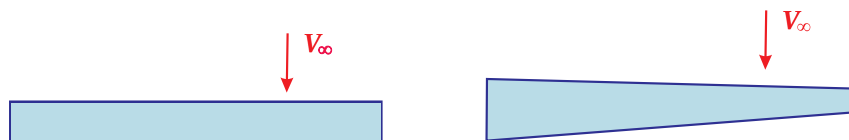
Figure 8. Wing configurations considered for the aeroelastic analysis.

American Institute of Aeronautics and Astronautics

Aeroelastic case 1: straight wing

Stream Velocity : 40 m/s $\alpha = 1\ deg$ NASTRAN: 9.1500

N_{EL}	EBBM	TBM	$N = 1$	$N = 2$	$N = 3$	$N = 4$
2	8.8074	8.8076	8.8123	8.5268	8.7961	8.8019
5	8.8073	8.8075	8.8122	8.7092	9.0097	9.0243
10	8.8073	8.8075	8.8122	8.7685	9.0710	9.0895
20	8.8072	8.8075	8.8122	8.7980	9.1012	9.1209
40	8.8071	8.8075	8.8122	8.8126	9.1164	9.1369

Table 5. Convergence study: Effect of the number of B4 elements on $u_{z\,\max}$ $[mm]$. Aerodynamic mesh: 6×60 VLM panels. Symmetry enabled.

Aeroelastic case 1: straight wing

Stream Velocity : 40 m/s $\alpha = 1\ deg$

N_{PANELS}	EBBM	TBM	$N = 1$	$N = 2$	$N = 3$	$N = 4$	NASTRAN
2×20	8.9903	8.9904	8.9953	8.9936	9.3029	9.3231	9.3253
4×40	8.8545	8.8546	8.8594	8.8473	9.1521	9.1719	9.2004
6×60	8.8072	8.8075	8.8122	8.7980	9.1012	9.1209	9.1500
10×100	8.7679	8.7681	8.7727	8.7565	9.0585	9.0781	9.1083

Table 6. Convergence study: Effect of the number of aerodynamic VLM panels on $u_{z\,\max}$ $[mm]$. Structural mesh: 20 elements B4. Symmetry enabled.

Aeroelastic case 2: straight wing with dihedral

Stream Velocity : 40 m/s $\alpha = 1\ deg$ NASTRAN: 11.2659

N_{EL}	EBBM	TBM	$N = 1$	$N = 2$	$N = 3$	$N = 4$
2	10.7476	10.7478	10.7543	10.5085	10.8235	10.8303
5	10.7475	10.7476	10.7542	10.7334	11.0902	11.1071
10	10.7471	10.7474	10.7542	10.8063	11.1661	11.1880
20	10.7481	10.7488	10.7542	10.8425	11.2033	11.2268
40	10.7549	10.7535	10.7542	10.8606	11.2220	11.2465

Table 7. Convergence study: Effect of the number of B4 elements on $u_{z\,\max}$ $[mm]$. Aerodynamic mesh: 6×60 VLM panels. Symmetry enabled.

American Institute of Aeronautics and Astronautics

Aeroelastic case 2: straight wing with dihedral

Stream Velocity : 40 m/s $\alpha = 1 \ deg$

N_{PANELS}	EBBM	TBM	$N=1$	$N=2$	$N=3$	$N=4$	NASTRAN
2×20	10.9702	10.9710	10.9766	11.0845	11.4524	11.4765	11.4779
4×40	10.8050	10.8057	10.8114	10.9033	11.2658	11.2894	11.3277
6×60	10.7481	10.7488	10.7542	10.8425	11.2033	11.2268	11.2659
10×100	10.7000	10.7011	10.7063	10.7914	11.1507	11.1740	11.2148

Table 8. Convergence study: Effect of the number of aerodynamic VLM panels on $u_{z\,\max}$ [mm]. Structural mesh: 20 elements B4. Symmetry enabled.

Aeroelastic case 3: swept tapered wing

Stream Velocity : 40 m/s $\alpha = 1 \ deg$ NASTRAN: 6.3806

N_{EL}	EBBM	TBM	$N=1$	$N=2$	$N=3$	$N=4$
2	6.4814	6.4816	6.4837	6.1732	6.5183	6.5282
5	6.1779	6.1780	6.1800	6.0000	6.3359	6.3505
10	6.1352	6.1354	6.1373	6.0011	6.3344	6.3490
20	6.1246	6.1248	6.1267	6.0110	6.3464	6.3602
40	6.1220	6.1221	6.1240	6.0181	6.3542	6.3680

Table 9. Convergence study: Effect of the number of B4 elements on $u_{z\,\max}$ [mm]. Aerodynamic mesh: 6×60 VLM panels. Symmetry enabled.

Aeroelastic case 3: swept tapered wing

Stream Velocity : 40 m/s $\alpha = 1 \ deg$

N_{PANELS}	EBBM	TBM	$N=1$	$N=2$	$N=3$	$N=4$	NASTRAN
2×20	6.2274	6.2275	6.2295	6.1197	6.4629	6.4771	6.4791
4×40	6.1513	6.1514	6.1533	6.0386	6.3755	6.3894	6.4093
6×60	6.1246	6.1248	6.1267	6.0110	6.3464	6.3602	6.3806
10×100	6.1020	6.1022	6.1040	5.9875	6.3215	6.3354	6.3566

Table 10. Convergence study: Effect of the number of aerodynamic VLM panels on $u_{z\,\max}$ [mm]. Structural mesh: 20 elements B4. Symmetry enabled.

American Institute of Aeronautics and Astronautics

Figure 9. Aeroelastic deflection of the straight wing for case 1 ($\alpha = 1°$).

American Institute of Aeronautics and Astronautics

Deflection of the swept wing exposed to free stream with velocity V = 40 m/s   N = 4
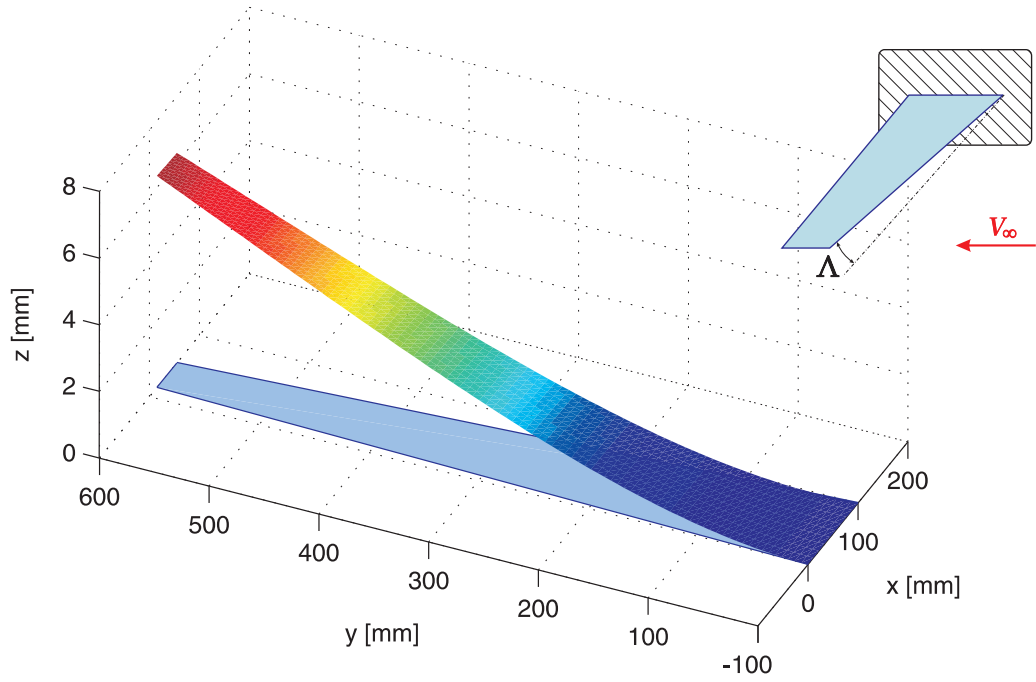

Figure 10.   Aeroelastic deflection of the swept tapered wing for case 3 ($\alpha = 1°$).

Torsional effect on the swept wing exposed to the free stream with velocity V = 40 m/s   N = 4

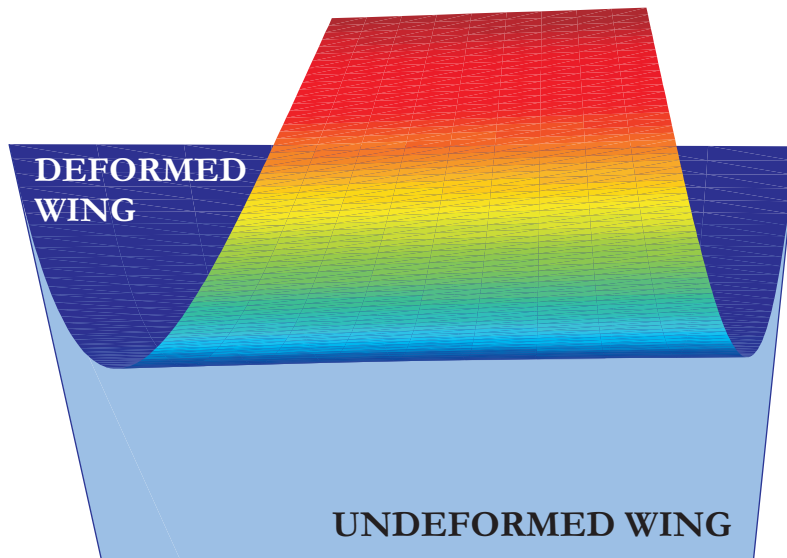**Figure 11.   Torsional effect on tip cross-section of the swept tapered wing.**

American Institute of Aeronautics and Astronautics

Appendix

The set of nine components of *fundamental nucleus* $\boldsymbol{K}^{ij\tau s}$ is written in a comprehensive form as:

$$
\begin{aligned}
K_{xx}^{ij\tau s} =\ & \widetilde{C}_{22} \int_{\Omega} F_{\tau,x}\, F_{s,x}\, d\Omega \int_{l} N_i\, N_j\, dy \ +\ \widetilde{C}_{26} \int_{\Omega} F_{\tau,z}\, F_{s,x}\, d\Omega \int_{l} N_i\, N_j\, dy\ + \\
& \widetilde{C}_{26} \int_{\Omega} F_{\tau,x}\, F_{s,z}\, d\Omega \int_{l} N_i\, N_j\, dy \ +\ \widetilde{C}_{66} \int_{\Omega} F_{\tau,z}\, F_{s,z}\, d\Omega \int_{l} N_i\, N_j\, dy\ + \\
& \widetilde{C}_{44} \int_{\Omega} F_{\tau}\, F_{s}\, d\Omega \int_{l} N_{i,y}\, N_{j,y}\, dy
\end{aligned}
$$

$$
\begin{aligned}
K_{xy}^{ij\tau s} =\ & \widetilde{C}_{23} \int_{\Omega} F_{\tau,x}\, F_{s}\, d\Omega \int_{l} N_i\, N_{j,y}\, dy \ +\ \widetilde{C}_{36} \int_{\Omega} F_{\tau,z}\, F_{s}\, d\Omega \int_{l} N_i\, N_{j,y}\, dy\ + \\
& \widetilde{C}_{45} \int_{\Omega} F_{\tau}\, F_{s,z}\, d\Omega \int_{l} N_{i,y}\, N_j\, dy \ +\ \widetilde{C}_{44} \int_{\Omega} F_{\tau}\, F_{s,x}\, d\Omega \int_{l} N_{i,y}\, N_j\, dy
\end{aligned}
$$

$$
\begin{aligned}
K_{xz}^{ij\tau s} =\ & \widetilde{C}_{12} \int_{\Omega} F_{\tau,x}\, F_{s,z}\, d\Omega \int_{l} N_i\, N_j\, dy \ +\ \widetilde{C}_{16} \int_{\Omega} F_{\tau,z}\, F_{s,z}\, d\Omega \int_{l} N_i\, N_j\, dy\ + \\
& \widetilde{C}_{26} \int_{\Omega} F_{\tau,x}\, F_{s,x}\, d\Omega \int_{l} N_i\, N_j\, dy \ +\ \widetilde{C}_{66} \int_{\Omega} F_{\tau,z}\, F_{s,x}\, d\Omega \int_{l} N_i\, N_j\, dy\ + \\
& \widetilde{C}_{45} \int_{\Omega} F_{\tau}\, F_{s}\, d\Omega \int_{l} N_{i,y}\, N_{j,y}\, dy
\end{aligned}
$$

$$
\begin{aligned}
K_{yx}^{ij\tau s} =\ & \widetilde{C}_{45} \int_{\Omega} F_{\tau,z}\, F_{s}\, d\Omega \int_{l} N_i\, N_{j,y}\, dy \ +\ \widetilde{C}_{44} \int_{\Omega} F_{\tau,x}\, F_{s}\, d\Omega \int_{l} N_i\, N_{j,y}\, dy\ + \\
& \widetilde{C}_{23} \int_{\Omega} F_{\tau}\, F_{s,x}\, d\Omega \int_{l} N_{i,y}\, N_j\, dy \ +\ \widetilde{C}_{36} \int_{\Omega} F_{\tau}\, F_{s,z}\, d\Omega \int_{l} N_{i,y}\, N_j\, dy
\end{aligned}
$$

$$
\begin{aligned}
K_{yy}^{ij\tau s} =\ & \widetilde{C}_{55} \int_{\Omega} F_{\tau,z}\, F_{s,z}\, d\Omega \int_{l} N_i\, N_j\, dy \ +\ \widetilde{C}_{45} \int_{\Omega} F_{\tau,x}\, F_{s,z}\, d\Omega \int_{l} N_i\, N_j\, dy\ + \\
& \widetilde{C}_{45} \int_{\Omega} F_{\tau,z}\, F_{s,x}\, d\Omega \int_{l} N_i\, N_j\, dy \ +\ \widetilde{C}_{44} \int_{\Omega} F_{\tau,x}\, F_{s,x}\, d\Omega \int_{l} N_i\, N_j\, dy\ + \\
& \widetilde{C}_{33} \int_{\Omega} F_{\tau}\, F_{s}\, d\Omega \int_{l} N_{i,y}\, N_{j,y}\, dy
\end{aligned}
$$

$$
\begin{aligned}
K_{yz}^{ij\tau s} =\ & \widetilde{C}_{55} \int_{\Omega} F_{\tau,z}\, F_{s}\, d\Omega \int_{l} N_i\, N_{j,y}\, dy \ +\ \widetilde{C}_{45} \int_{\Omega} F_{\tau,x}\, F_{s}\, d\Omega \int_{l} N_i\, N_{j,y}\, dy\ + \\
& \widetilde{C}_{13} \int_{\Omega} F_{\tau}\, F_{s,z}\, d\Omega \int_{l} N_{i,y}\, N_j\, dy \ +\ \widetilde{C}_{36} \int_{\Omega} F_{\tau}\, F_{s,x}\, d\Omega \int_{l} N_{i,y}\, N_j\, dy
\end{aligned}
$$

$$
\begin{aligned}
K_{zx}^{ij\tau s} =\ & \widetilde{C}_{12} \int_{\Omega} F_{\tau,z}\, F_{s,x}\, d\Omega \int_{l} N_i\, N_j\, dy \ +\ \widetilde{C}_{26} \int_{\Omega} F_{\tau,x}\, F_{s,x}\, d\Omega \int_{l} N_i\, N_j\, dy\ + \\
& \widetilde{C}_{16} \int_{\Omega} F_{\tau,z}\, F_{s,z}\, d\Omega \int_{l} N_i\, N_j\, dy \ +\ \widetilde{C}_{66} \int_{\Omega} F_{\tau,x}\, F_{s,z}\, d\Omega \int_{l} N_i\, N_j\, dy\ + \\
& \widetilde{C}_{45} \int_{\Omega} F_{\tau}\, F_{s}\, d\Omega \int_{l} N_{i,y}\, N_{j,y}\, dy
\end{aligned}
$$

$$
\begin{aligned}
K_{zy}^{ij\tau s} =\ & \widetilde{C}_{13} \int_{\Omega} F_{\tau,z}\, F_{s}\, d\Omega \int_{l} N_i\, N_{j,y}\, dy \ +\ \widetilde{C}_{36} \int_{\Omega} F_{\tau,x}\, F_{s}\, d\Omega \int_{l} N_i\, N_{j,y}\, dy\ + \\
& \widetilde{C}_{55} \int_{\Omega} F_{\tau}\, F_{s,z}\, d\Omega \int_{l} N_{i,y}\, N_j\, dy \ +\ \widetilde{C}_{45} \int_{\Omega} F_{\tau}\, F_{s,x}\, d\Omega \int_{l} N_{i,y}\, N_j\, dy
\end{aligned}
$$

$$
\begin{aligned}
K_{zz}^{ij\tau s} =\ & \widetilde{C}_{11} \int_{\Omega} F_{\tau,z}\, F_{s,z}\, d\Omega \int_{l} N_i\, N_j\, dy \ +\ \widetilde{C}_{16} \int_{\Omega} F_{\tau,x}\, F_{s,z}\, d\Omega \int_{l} N_i\, N_j\, dy\ + \\
& \widetilde{C}_{16} \int_{\Omega} F_{\tau,z}\, F_{s,x}\, d\Omega \int_{l} N_i\, N_j\, dy \ +\ \widetilde{C}_{66} \int_{\Omega} F_{\tau,x}\, F_{s,x}\, d\Omega \int_{l} N_i\, N_j\, dy\ + \\
& \widetilde{C}_{55} \int_{\Omega} F_{\tau}\, F_{s}\, d\Omega \int_{l} N_{i,y}\, N_{j,y}\, dy
\end{aligned}
$$

American Institute of Aeronautics and Astronautics

References

[1]Livne E., Weisshaar T.A., "*Aeroelasticity of Nonconventional Airplane Configurations-Past and Future*", Journal of Aircraft, Vol. 40, No. 6, 2003, pp. 1047-1065.

[2]Frediani A., Rizzo E., Bottoni C., Scanu J., Iezzi G., "*A 250 Passenger Prandtlplane Transport Aircraft Preliminary Design*", Aerotecnica Missili e Spazio (AIDAA), Vol. 84, No. 4, September 2005.

[3]Livne E.,"*Future of Airplane Aeroelasticity*", Journal of Aircraft, Vol. 40, No. 6, 2003, pp. 1066-1092.

[4]Demasi L., Livne E., "*Exploratory Studies of Joined Wing Aeroelasticity*", 46th AIAA/ASME/ASCE/AHS/ASC Structures, Structural Dynamics, and Materials Conference, Austin, TX, AIAA Paper 2005-2172, April 2005.

[5]Patil M. J., Hodges D. H. and Cesnik C. E. S., "*Nonlinear Aeroelasticity and Flight Dynamics of High-Altitude Long-Endurance Aircraft*", Journal of Aircraft, Vol. 38, No. 1, 2001, pp. 88-94.

[6]Patil M. J., Hodges D. H. and Cesnik C. E. S., "*Limit Cycle Oscillations in High-Aspect-Ratio Wings*", Journal of Fluids and Structures, Vol. 15, No. 1, 2001, pp. 107-132.

[7]Sulaeman E., Kapania R. and Haftka R. T., "*Parametric Studies of Flutter Speed in a Strut-braced Wing*", 43rd AIAA/ASME/ASCE/AHS/ASC Structures, Structural Dynamics, and Materials Conference, Denver, CO, AIAA Paper 2002-1487, April 2002.

[8]Sulaeman E., "*Effect of Compressive Force on Aeroelastic Stability of a Strut-Braced Wing*", Ph.D Dissertation, Virginia Polytechnic Inst. and State Univ., Blacksburg, VA, November 2001.

[9]Bhatia M., Kapania K., Van Hoek M. and Haftka R., "*Structural Design of a Truss Braced Wing: Potential and Challenges*", 50rd AIAA/ASME/ASCE/AHS/ASC Structures, Structural Dynamics, and Materials Conference, Palm Springs, CA, AIAA Paper 2009-2147, May 2009.

[10]Demasi L., Livne E., "*Aeroelastic Coupling of Geometrically Nonlinear Structures and Linear Unsteady Aerodynamics: Two formulations*", Journal of Fluids and Structures, Vol. 25, 2009, pp. 918-935.

[11]Hodges D. H., "*A Mixed Variational Formulation Based on Exact Intrinsic Equations for Dynamics of Moving Beams*", International Journal of Solids and Structures, Vol. 26, No. 11, 1990, pp. 1253-1273.

[12]Kapania K., Raciti S., "*Recent Advances in Analysis of Laminated Beams and Plates, Part I: Shear Effects and Buckling*", AIAA Journal, Vol. 27, No. 7, 1989, pp. 923-935.

[13]Kapania K., Raciti S., "*Recent Advances in Analysis of Laminated Beams and Plates, Part II: Vibrations and Wave Propagation*", AIAA Journal, Vol. 27, No. 7, 1989, pp. 935-946.

[14]Kim G., White S. R., "*Thick-Walled Composite Beam Theory Including 3D Elastic Effects and Torsional Warping*", International Journal of Solid Structures, Vol. 34, No. 31-32, 1997, pp. 4237-4259.

[15]Reddy J. N., "*On Locking-Free Shear Deformable Beam Finite Elements*", Computer Methods in Applied Mechanics and Engineering, Vol. 149, 1997, pp. 113-132.

[16]Lee. J., "*Flexural Analysis of Thin-Walled Composite Beams Using Shear-Deformable Beam Theory*", Composite Structures, Vol. 70, No. 2, 2005, pp. 212-222.

[17]Volovoi V. V., Hodges D. H., Berdichevsky V. L. and Sutyrin V. G., "*Asymptotic Theory for Static Behavior of Elastic Anisotropic I-beams*", International Journal of Solid Structures, Vol. 36, 1999, pp. 1017-1043.

[18]Volovoi V. V., Hodges D. H., "*Theory of Anisotropic Thin-Walled Beams*", Journal of Applied Mechanics, Vol. 67, 2000, pp. 453-459.

[19]Yu W., Volovoi V. V., Hodges D. H., and Hong X., "*Validation of the Variational Asymptotic Beam Sectional Analysis (VABS)*", AIAA Journal, Vol. 40, No. 10, 2002, pp. 2105-2113.

[20]Carrera E., "*Theories and Finite Elements for Multilayered Plates and Shells: a Unified Compact Formulation with Numerical Assessment and Benchmarking*", Archives of Computational Methods in Engineering, Vol. 10, No. 3, 2003, pp. 215-296.

[21]Reddy J. N., "*Mechanics of Laminated Composite Plates and Shells. Theory and Analysis*", CRC Press, 2nd Edition, Florida, 2004.

[22]Jones R., "*Mechanics of Composite Materials*", Taylor & Francis, 2nd Edition, Philadelphia, PA, 1999.

[23]Timoshenko S., "*Strength of Materials*", Van Nostrand company, New York, 1940.

[24]Carrera E., Brischetto S. , "*Analysis of Thickness Locking in Classical, Refined and Mixed Multilayered Plate Theories*", Composite Structures, Vol. 82, No. 4, 2008, pp. 549-562.

[25]Carrera E., Brischetto S., "*Analysis of Thickness Locking in Classical, Refined and Mixed Theories for Layered Shells*", Composite Structures, Vol. 85, No. 1, 2008, pp. 83-90.

[26]Giunta G., Carrera E. and Belouettar S., "*A Refined Beam Theory with only Displacement Variables and Deformable Cross-Section*", 50th AIAA/ASME/ASCE/AHS/ASC Structures, Structural Dynamics, and Materials Conference, Palm Springs, CA, AIAA Paper 2009-2370, May 2009.

[27]Carrera E., Demasi L., "*Classical and Advanced Multilayered Plate Elements Based upon PVD and RMVT. Part 1: Derivation of Finite Element Matrices*", International Journal for Numerical Methods in Engineering, Vol. 55, 2002, pp. 191-231.

[28]Carrera E., Demasi L., "*Classical and Advanced Multilayered Plate Elements Based upon PVD and RMVT. Part 2: Numerical Implementations*", International Journal for Numerical Methods in Engineering, Vol. 55, 2002, pp. 253-291.

[29]Carrera E., Giunta G., Nali M. and Petrolo M., "*Refined Beam Elements with Arbitrary Cross-Section Geometries*", Computers and Structures, Vol. 88, No. 5-6, 2009, pp. 283-293.

[30]Carrera E., Petrolo M. and Nali M., "*Unified Formulation Applied to Free Vibrations Finite Element Analysis of Beams with Arbitrary Section*", Shock and Vibration, in press, 2010.

[31]Bathe K.J., "*Finite Element Procedure*", Prencite Hall, New Jersey, July 1995.

[32]Demasi L., Livne E., "*Dynamic Aeroelasticity of Structural Nonlinear Configurations Using Linear Modally Reduced Aerodynamic Generalized Forces*", AIAA Journal, Vol. 47, No. 1, 2009, pp. 71-90.

American Institute of Aeronautics and Astronautics

[33]Harder R., MacNeal R. and Rodden W., "*A Design for the Incorporation of Aeroelastic Capability into NASTRAN*", report NASA N71-33303, May 1977.

[34]Rodden W., Harder R. and Bellinger D., "*Aeroelastic Addiction to NASTRAN*", NASA contractor report 3094, March 1979.

[35]Harder R., Desmarais R. N., "*Interpolation Using Surface Splines*", Journal of Aircraft, Vol. 9, No. 2, 1972, pp. 189-192.

[36]ZONA Technology, Inc., "*Spline Methods for Spline Matrix Generation*", ZAERO Theoretical Manual, Ver. 7.1, 2004.

[37]MacNeal-Schwendler corp., "*Interconnection of the Structure with Aerodynamics*", MSC.NASTRAN Theoretical Manual, Ver. 68, Los Angeles, CA, 1994.

[38]Katz J., Plotkin A., "*Low-Speed Aerodynamics*", McGraw-Hill, New York, 1991.